

# Magnetic structure determination of $\text{TbCo}_2\text{Ni}_3$ using polarized and nonpolarized neutron powder diffraction

Oleg Rivin\*

Department of Physics, Nuclear Research Centre-Negev, P.O. Box 9001, Beer Sheva 84190, Israel  
and Department of Physics, Ben-Gurion University, P.O. Box 653, Beer Sheva 84105, Israel

El'ad N. Caspi and Hanania Ettetdgui

Department of Physics, Nuclear Research Centre-Negev, P.O. Box 9001, Beer Sheva 84190, Israel

Hagai Shaked

Department of Physics, Ben-Gurion University, P.O. Box 653, Beer Sheva 84105, Israel

Arsen Gukasov

Laboratoire Léon Brillouin, CEA-CNRS, CE Saclay, 91191 Gif sur Yvette, France

(Received 30 April 2013; revised manuscript received 23 June 2013; published 30 August 2013)

The structural (space group  $P6/mmtn$ ) and magnetic parameters of  $\text{TbCo}_2\text{Ni}_3$  are investigated using neutron powder diffraction and polarized neutron powder diffraction at several temperatures below the magnetic transition temperature. It is found that this compound orders ferrimagnetically at 315 K, with ferromagnetic Tb and Co/Ni sublattices. Below 100 K, the magnetic axis is perpendicular to the hexagonal axis. Above 100 K, the magnetic axis reorients slightly towards the hexagonal axis. The magnitudes and orientation of the ordered magnetic moments exhibit complex temperature dependences. The observed magnitude of the ordered Tb magnetic moment at  $T = 10$  K, is found to be  $8.1(2) \mu_B$ , smaller than the free  $\text{Tb}^{3+}$  ion. The significance of this property, and its relation to the mechanisms driving the magnetic order in the parent  $\text{TbCo}_5$  compound, are discussed.

DOI: [10.1103/PhysRevB.88.054430](https://doi.org/10.1103/PhysRevB.88.054430)

PACS number(s): 75.50.-y, 61.05.fm

## I. INTRODUCTION

The  $R\text{Co}_5$  ( $R = \text{lanthanides}$ ) compounds attracted great experimental and theoretical interest for many years for both technological importance and basic research.<sup>1-5</sup> These compounds crystallize in hexagonal  $\text{CaCu}_5$  type<sup>1</sup> structure with  $P6/mmm$  space group symmetry. They undergo magnetic ordering at high Curie temperatures ( $\sim 1000$  K) with very large magnetocrystalline anisotropy (MCA).<sup>2,3</sup> The Co atoms occupy two nonequivalent crystallographic Fig. 1 sites,  $2c$  ( $\bar{6}m2$ ) and  $3g$  ( $mmm$ ), which exhibit different MCAs.<sup>3,5</sup> In particular, the very large MCA, along the unique hexagonal  $c$  axis, originates from the  $2c$  site, while that of the  $3g$  site is much smaller and favors the hexagonal plane. The  $R$  atom occupies the  $1a$  site. For  $R = \text{Tb}$ , the MCA is perpendicular to the  $c$  axis.<sup>3</sup>

The combined actions of the magnetic exchange field (MEF) and the crystalline electric field (CEF) strongly affect the magnetism in the  $R\text{Co}_5$  compounds and their derivatives. In  $\text{TbCo}_3\text{B}_2$ , this combined action leads to a self-induced magnetic ordering transition.<sup>6</sup> The theory of this type of transition was investigated thoroughly.<sup>7</sup> Basically, this transition evolves from  $R$  ions (i.e., Tb), whose ground level (determined by the CEF) is a nonmagnetic singlet (Van-Vleck paramagnet). A small magnetic field induces, by admixture of higher levels, a small magnetic moment into the ground level. These small moments increase, and (consequently) the MEF increases as temperature decreases until a critical MEF value is reached, at which long-range magnetic order takes place. The effect of the  $3d$  (i.e., Co) sublattice on this transition enters through its contribution to the MEF at the  $R$  site.<sup>6,7</sup>

Partial substitution of the Co by  $A$  in the ternary compounds  $R(\text{Co}_{1-x}\text{A}_x)_5$  ( $A = \text{Ni, Fe, Al, Cu}$ ) enables a gradual change in the MEF, originating from the Co sublattices, without altering the crystal structure. It was found using experiments and theoretical calculations that the magnetic properties are related to the type and amount of  $A$  substitution.<sup>8-11</sup> Hence, the gradual reduction of this dominant exchange field allows the study of the mechanisms responsible for the following properties: MCA, ordering temperature, magnitude of ordered magnetic moment, and its direction with respect to the crystal axes.<sup>11-14</sup> Also, it is already known that the ground levels of  $\text{Tb}^{3+}$  in  $\text{TbCo}_3\text{B}_2$  (Ref. 6) and in  $\text{TbNi}_5$  (Ref. 15) are nonmagnetic singlets. Hence, we suggest that these CEF- and MEF-driven mechanisms in  $R(\text{Co}_{1-x}\text{Ni}_x)_5$  lead to self-induced magnetic transition on the  $R$  sublattice, similar to the one found in  $\text{TbCo}_3\text{B}_2$ .<sup>6,7</sup> The present study of  $\text{Tb}(\text{Co}_{1-x}\text{Ni}_x)_5$  with  $x = 0.6$  is motivated by this idea.

In order to avoid the need for high-temperature equipment,  $x$  is chosen in the present work so that  $T_c$  is decreased from  $\sim 1000$  K ( $x = 0$ ) to  $\sim 300$  K ( $x > 0$ ). Following the results obtained for  $\text{Y}(\text{Co}_{1-x}\text{Ni}_x)_5$ ,<sup>12</sup> the value  $x = 0.6$  was chosen. Also, for this value, it is expected that the magnitude of the ordered magnetic moments on the  $2c$  and  $3g$  sites would be about  $1 \mu_B$ . This moment's magnitude allows sufficient experimental sensitivity to measure the Co moment temperature dependence. Hence, in the present work, we studied the local (microscopic), structural, and magnetic parameters of  $\text{TbCo}_2\text{Ni}_3$ , and their temperature dependence, using neutron powder diffraction (NPD) and polarized neutron powder diffraction (PNPD).

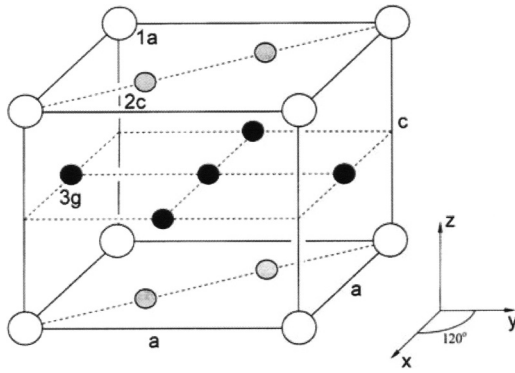


FIG. 1. The  $\text{CaCu}_5$  type crystallographic structure of  $\text{RCu}_5$ , in which the  $R$  sublattice consists of the  $1a$  site and the Co sublattices consist of the  $2c$  and the  $3g$  sites.

The experimental details and procedure of sample preparation, x-ray diffraction (XRD), ac susceptibility, NPD, and PNPd at various temperatures are described in Sec. II. The experimental results and their analysis are presented in Sec. III. The final results and discussion are given in Sec. IV. The conclusions drawn from the present work are summarized in Sec. V.

## II. EXPERIMENTAL

Polycrystalline  $\text{TbCo}_2\text{Ni}_3$  was prepared in an arc melting furnace using high-purity elements (99.9%). The sample was remelted five times in an Ar-controlled environment, followed by an anneal for 20 d at  $720^\circ\text{C}$ . The crystallographic structure was characterized using x-ray powder diffraction, using  $\text{Cu } K_\alpha$  radiation.

Measurements of ac magnetic susceptibility were carried out from 325 K down to 5 K on a 58-mg  $\text{TbCo}_2\text{Ni}_3$  specimen taken from the sample. The amplitude of the applied ac ( $f \sim 1.5$  kHz) magnetic field was 10 Oe. Liquid He was used for cooling. Calibration of the ac susceptometer was done in the temperature range  $78 \text{ K} < T < 300 \text{ K}$  using a 42-mg powder sample of  $\text{Ho}_2\text{O}_3$  (room temperature molar susceptibility  $\chi_M \sim 89 \times 10^{-3}$  emu/mole).

Neutron powder diffraction measurements were performed at the following temperatures: 10, 50, 100, and 298 K. The measurements were carried out at the KARL powder double-axis diffractometer in Israel Research Reactor No. 1 (IRR-1) at the Nuclear Research Center, Soreq, Israel (Israel Atomic Energy Commission). The KARL diffractometer, originating from the Physikalisch-Technische Bundesanstalt (PTB) Braunschweig reactor, was recently set up at IRR-1.<sup>16</sup> The diffractometer and its 14  $^3\text{He}$ -based neutron multidetectors were calibrated using various standard powder samples ( $\text{Al}_2\text{O}_3$ , Si, and Ag). The incident neutron beam [ $\lambda = 0.982(1)$  Å] was obtained from the (110) reflection of a copper single-crystal monochromator. A low value of  $\lambda$  was preferred for the crystallographic study. An angular step of  $0.05^\circ$ , combined with a small mosaicity ( $\sim 0.25^\circ$ ) of the monochromating single crystal, was chosen to achieve medium angular resolution, compared with other powder machines.<sup>17</sup> A 15-g  $\text{TbCo}_2\text{Ni}_3$  powder sample was loaded into a vanadium cylindrical sample holder, with a 10-mm diameter and  $\sim 0.2$ -mm wall thickness.

Vanadium was used to reduce coherent scattering from the sample holder.

Polarized neutron powder diffraction experiments were performed at the following temperatures: 10, 50, 100, 150, 175, and 200 K. The measurements were carried out at the Very Intense Polarized (VIP; former 5C1) diffractometer<sup>18</sup> at the Orphée research reactor at the Laboratoire Léon Brillouin (Commissariat à l’Energie Atomique et aux Energies Alternatives [CEA]—Centre National de la Recherche Scientifique [CNRS]) Saclay, France. A monochromatic  $\lambda = 0.84(1)$  Å and polarized  $P = 0.88(1)$  incident neutron beam was obtained using the Heusler crystal ( $\text{Cu}_2\text{MnAl}$ ) method.<sup>19</sup> A cryoflipper, installed between the Heusler crystal and the sample, was used for the neutron spin reversal with respect to the externally applied magnetic field  $H_0$ . The scattered neutrons were detected using a two-dimensional (2D) position-sensitive  $^3\text{He}$  detector, limiting the measured neutrons to a vertical acceptance angle of  $-5^\circ$  to  $5^\circ$  about the scattering plane, perpendicular to  $H_0$ . The experimental results, thus obtained, underwent a smoothing procedure due to irregular steps in the measured scattering angle  $2\theta$  by the detector. The smoothing procedure was performed in the standard linear extrapolations routine in the FULLPROF<sup>20</sup> program, utilizing 10 cycles. A 10.4(1)-g  $\text{TbCo}_2\text{Ni}_3$  powder sample was loaded into a  $\text{Ti}_{0.522}\text{Zr}_{0.478}$  (Ti/Zr) cylindrical sample holder with a 5-mm diameter and  $\sim 0.2$ -mm wall thickness. A Ti/Zr holder was used to reduce possible coherent scattering from the holder.<sup>21</sup> The loaded sample holder was placed in an external magnetic field  $H_0$  of 5 T to achieve saturation magnetization at different sample temperatures. The  $H_0$  direction is perpendicular to the horizontal scattering plane and pointing up (+). The PNPd experiment yields the observed neutron count rates  $I_+$  and  $I_-$  at scattering angle  $2\theta$  with the incident neutron beam polarized parallel and antiparallel to the external magnetic field direction, respectively. In practice, these count rates are represented by the neutron count collected per  $2\theta$  channel per prefixed beam monitor counts.

Both XRD and NPD data were analyzed using the Rietveld refinement method with the FULLPROF code.<sup>20</sup> The PNPd data were analyzed using a computer routine “PolCalc” (Sec. III D) created for this work. This routine refines the crystallographic and magnetic parameters to best fit the entire body of PNPd data.

## III. RESULTS AND ANALYSIS

### A. Crystal structure—XRD

A  $\text{CaCu}_5$  type structure, Fig. 1, is identified using XRD, Fig. 2. An impurity structure,  $\text{TbO}_\delta$  ( $\delta \approx 1.6$ ), found at the arc melted sample disappeared after the annealing process. The lattice parameters, which were refined to fit the observed profile of the annealed specimen, Fig. 2(b), are  $a = 4.916(1)$  and  $c = 3.975(2)$  Å.

### B. ac susceptibility

The molar ac susceptibility  $\chi_M$  of  $\text{TbCo}_2\text{Ni}_3$  as a function of temperature (Fig. 3) shows a magnetic transition temperature  $T_C \sim 315$  K. Below  $T_C$ , a behavior reminiscent of long-range magnetic order is observed. The observed, complex, magnetic

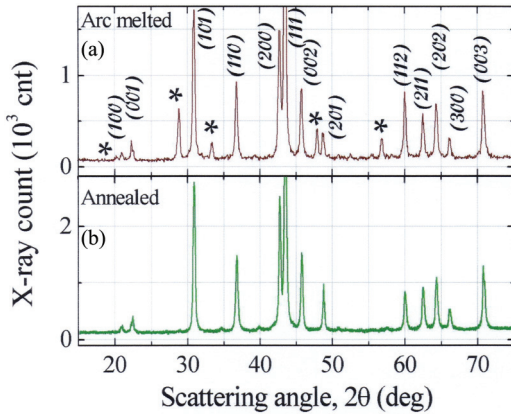


FIG. 2. (Color online) Observed XRD (Cu  $K\alpha$  radiation) profile of  $\text{TbCo}_2\text{Ni}_3$  specimen. (a) Arc melted prior to annealing. The Miller indices correspond to a  $\text{CaCu}_5$  type ( $P6/mmm$ ) unit cell (Table I). The asterisks mark five  $\text{TbO}_3$  impurity lines. (b) Annealed.

response curve at  $T < T_C$  is assumed to be the result of a superposition between the magnetic responses of the Tb and Co/Ni sublattices.

The previously published<sup>22,23</sup>  $T_C$ - $x$  dependence in  $\text{Tb}(\text{Co}_{1-x}\text{Ni}_x)_5$  (Fig. 4) with  $T_C$  value obtained in the present work (solid triangle) is shown for comparison with the observed  $T_C$ - $x$  dependence in  $\text{Y}(\text{Co}_{1-x}\text{Ni}_x)_5$ .<sup>12</sup> No magnetic ordering transition is present in  $\text{Y}(\text{Co}_{1-x}\text{Ni}_x)_5$  for  $0.7 < x$ , while  $\text{Tb}(\text{Co}_{1-x}\text{Ni}_x)_5$  exhibits magnetic ordering transition up to  $x = 1$ . Furthermore,  $T_C$  in  $\text{Tb}(\text{Co}_{1-x}\text{Ni}_x)_5$  appears to be higher than that of  $\text{Y}(\text{Co}_{1-x}\text{Ni}_x)_5$ . Hence, the magnetic ordering in  $\text{Tb}(\text{Co}_{1-x}\text{Ni}_x)_5$  compounds is enhanced by the interaction between the Tb and Co/Ni sublattices.

### C. NPD analysis

The NPD data at 298 K (room temperature) were analyzed using Rietveld's refinement method with the  $P6/mmm$  space group and the atomic positions specified in Table I, and yielded the structural and magnetic parameters in Table II. The NPD refined lattice parameters  $a = 4.909(3)$  and  $c = 3.977(5)$  Å are in good agreement with their XRD refined parameters

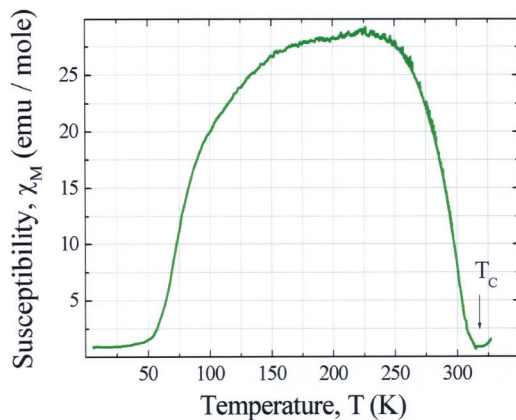


FIG. 3. (Color online) The ac molar susceptibility  $\chi_M$  (green) for  $\text{TbCo}_2\text{Ni}_3$  as a function of temperature. The magnetic transition temperature  $T_C$  is  $\sim 315$  K.

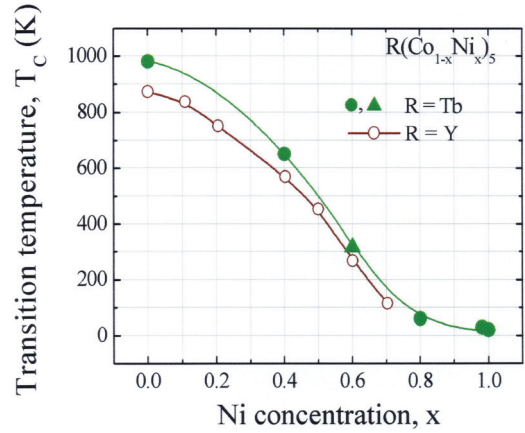


FIG. 4. (Color online) The  $T_C$  values observed for  $\text{Tb}(\text{Co}_{1-x}\text{Ni}_x)_5$  (solid symbols: circles from Refs. 2, 22, and 23; triangle from present work) and  $\text{Y}(\text{Co}_{1-x}\text{Ni}_x)_5$  (Ref. 12; open circles). The estimated  $T_C$  interpolation in  $\text{Tb}(\text{Co}_{1-x}\text{Ni}_x)_5$  assuming similarity to the  $R = \text{Y}$  curve, for  $0 < x < 0.6$  (dashed line).

(Sec. III A). As the sample is cooled, a significant intensity increase in some of the NPD lines (e.g., 100, 001, and 101) is observed (Fig. 5). This intensity increase indicates the emergence of a long-range (ferromagnetic or ferrimagnetic) order which corresponds to the increase in the magnetic response observed with the ac susceptometer below  $\sim 315$  K (Fig. 3). Possibly, an anomalous thermal expansion of the  $c$  lattice parameter is observed (Table II) at 298 K near  $T_C$ , similar to previously found<sup>23</sup> anomalies in  $RCO_5$ .

In refining the crystallographic and magnetic parameters to fit the observed diffraction patterns, a collinear magnetic structure was considered. In this model, the Tb (at  $1a$ ), Co/Ni (at  $2c$ ) and Co/Ni (at  $3g$ ) sublattices are each ferromagnetic and aligned parallel or antiparallel to the common magnetic axis. This magnetic axis is oriented with an inclination angle  $\Theta$  to the hexagonal unique axis ( $c$  axis; Fig. 1). This model allows four possible collinear configurations for magnetic ordering (Table III). The configuration found to best fit the observed NPD and PNP (Sec. III D) profiles is the  $D$  configuration, where the Tb sublattice ( $1a$ ) is antiparallel to the Co/Ni ( $2c$  and  $3g$ ) sublattices, as was found<sup>2,24,25</sup> in other  $RCO_5$  compounds, with 'heavy' Lanthanides, and  $\text{TbCo}_3\text{B}_2$ .

A non- $c$  axis component of the magnetic moment does not conform with hexagonal symmetry and will require a

TABLE I. The two model unit cells of the  $P6/mmm$  and  $Cmmm$  lattices and their atomic sites. The unit cells are defined with respect to the primitive lattice vectors of  $P6/mmm$ . All atoms sites are fixed by symmetry, except that of site  $4g$ , which was refined to  $0.35(3)$ .

Space group		$P6/mmm$ (191)	$Cmmm$ (65)
Unit cell basis	$a$	{1,0,0}	{2,1,0}
	$b$	{0,1,0}	{0,1,0}
	$c$	{0,0,1}	{0,0,1}
Coordinates	Tb	$1a$ : (0,0,0)	$2a$ : (0,0,0)
	Co/Ni	$3g$ : (1/2,0,1/2)	$2c$ : (1/2,0,1/2)
			$4f$ : (1/4,1/4,1/4)
	Co/Ni	$2c$ : (1/3,2/3,0)	$4g$ : (0.35,0,0)

TABLE II. Refined NPD values of structural and magnetic parameters of  $\text{TbCo}_2\text{Ni}_3$  at temperatures  $T = 10, 50, 100, 150,$  and  $298$  K. The structural refinement was carried using the  $P6/mmm$  space group;  $a$  and  $c$  are lattice parameters;  $B_{\text{Tb}}, B_{2c},$  and  $B_{3g}$  are the isotropic thermal factors at the Tb ( $1a$ ), Co/Ni ( $2c$ ), and Co/Ni ( $3g$ ) sites, respectively. PSO is of Co at  $2c$  (see text);  $\mu_{\text{Tb}}, \mu_{2c},$  and  $\mu_{3g}$  are the ordered magnetic moments at Tb ( $1a$ ), Co/Ni ( $2c$ ), and Co/Ni ( $3g$ ) sites, respectively. Here,  $\Theta$  is the angle between the magnetic and hexagonal axes. Also,  $\chi^2, R_p,$  and  $R_{wp}$  are the reliability factors, weighted profile factor, and the weighted square difference.<sup>20,27</sup> Numbers in parentheses are standard deviations of the last significant digit. Parameters lacking standard deviation were fixed throughout the refinement process.

$T(K)$	10	50	100	150	298
Parameter					
$a$ (Å)	4.909(3)	4.911(5)	4.915(3)	4.915(5)	4.916(4)
$c$ (Å)	3.977(5)	3.978(7)	3.980(4)	3.983(8)	3.974(4)
$B_{\text{Tb}}$ (Å <sup>2</sup> )	≈0	≈0	0.3(1)	0.3	0.5(1)
$B_{2c}$ (Å <sup>2</sup> )	0.3(1)	0.4(1)	0.4(1)	0.4	0.5(1)
$B_{3g}$ (Å <sup>2</sup> )	≈0	≈0	0.15(9)	0.15	0.2(1)
PSO	-0.4(1)	-0.4	-0.4	-0.4	-0.4
$\mu_{\text{Tb}}$ ( $\mu_B$ )	8.3(5)	7.1(8)	6.3(8)	4.0(8)	1.0(4)
$\mu_{2c}$ ( $\mu_B$ )	-1.0(1)	-1.1(2)	-0.9(1)	-0.8(2)	-0.8(4)
$\mu_{3g}$ ( $\mu_B$ )	-1.2(1)	-0.7(2)	-1.1(2)	-1.1(3)	-0.8(4)
$\Theta$ (deg)	90(10)	90(10)	90(10)	90(10)	— <sup>a</sup>
$\chi^2$	1.3	2.0	1.4	1.9	1.3
$R_p$	8.1	12	9	11	5.5
$R_{wp}$	10	16	12	15	7.0

<sup>a</sup>The magnetic reflections at 298 K were too weak (compared with the nuclear) to determine  $\Theta$ .

symmetry decrease. The expected symmetries are  $P6/mmm,$   $Cmmm,$  and  $C2/m,$  for  $\Theta = 0^\circ, \Theta = 90^\circ,$  and  $0^\circ < \Theta < 90^\circ,$  respectively.<sup>24-26</sup> This type of crystal symmetry decrease was reported in  $RCO_3B_2,$  where an orthorhombic distortion was observed.<sup>25</sup> Therefore, with  $0^\circ < \Theta < 90^\circ,$  a crystal symmetry decrease must be considered. In the present work,  $\Theta$  was found to be  $90^\circ$  for  $T < 100$  K, within the experimental precision, introducing the possibility of an orthorhombic distortion. Hence, two models, in which the crystallographic structure is either  $P6/mmm$  or  $Cmmm$  (henceforth hexagonal

or orthorhombic), were considered in order to find which crystallographic space group best fits the observed NPD profiles.

Each one of the two models was introduced to the refinement as a second phase, using the  $P1$  space group. Both models yielded similar refined magnetic structure parameters (magnitude and direction). The  $Cmmm$  refinement (where  $a$  and  $b$  lattice parameters were refined without constraint; Table I) did not give a significant improvement over the  $P6/mmm$  refinement, within the experimental precision. Therefore, the refined magnetic structures for all temperatures (Table II) were obtained using the  $D$  magnetic configuration (Table III), with the  $P6/mmm$  space group. The magnitude of the total magnetic moment in the unit cell  $\mu_{\text{tot}} = \mu_{\text{Tb}} + \mu_{2c} + \mu_{3g}$  are nearly saturated for  $T < 100$  K, in agreement with ac susceptibility results (Fig. 3).

In the case of random distribution of the Co and Ni ions in the  $2c$  and  $3g$  sites, the site occupancy of Co and Ni is  $2/5$  and  $3/5,$  respectively, in each of the two sites. This is the case of no preferred site occupancy (PSO). The Co occupancy at  $2c$  is given by (Co random occupancy)  $\times$  (1 + PSO). This relationship determines the Co and Ni occupancies at  $2c$  and  $3g$  sites (Table IV). Refinement to fit the 10 K data of the site occupancies yielded 0.24(4) for Co ion at site  $2c.$  Using the latter relationship,  $2/5 \times (1 + \text{PSO}),$  one obtains  $\text{PSO} = -0.4(1).$  This value was then fixed throughout the refinements to fit the data of the other temperatures. Preferred site occupancy was also reported in other  $R(\text{Co}_{1-x}\text{A}_x)_5$  ( $A = \text{Ga}, \text{Si}, \text{Cu}, \text{Al}$ ) compounds<sup>8,9</sup> and is directly related to the magnetic properties.

#### D. PNP analysis

The flipping difference (FD) intensity of the PNP  $I_+ - I_-$ <sup>28,29</sup> eliminates all nonmagnetic background (i.e., nuclear scattering, scattering from the cryomagnet, multiple

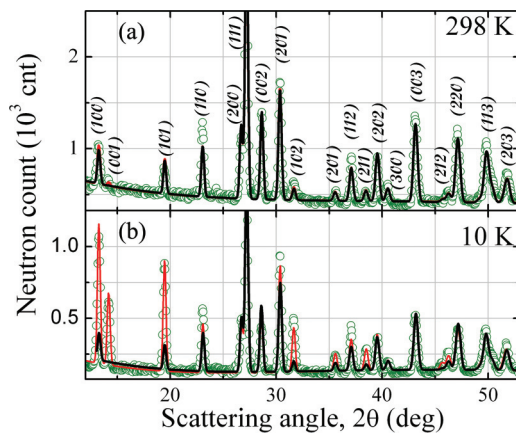


FIG. 5. (Color online) NPD of  $\text{TbCo}_2\text{Ni}_3$  at (a) 298 K and (b) 10 K. The circle symbols are the observed NPD data, the solid black and red lines are the calculated (refined using Rietveld's algorithm; Ref. 20) nuclear and the sum of nuclear and magnetic profiles, respectively. The reflections in (a) are marked by their Miller ( $P6/mmm$ ) indices. The emergence of considerable magnetic contributions to several reflections (i.e., 100, 001, 101, 201, and 102) at 10 K is apparent. These contributions indicate a ferro- or ferrimagnetic order at this temperature.

TABLE III. The four magnetic configurations allowed by the model where each of the Tb (*1a*), Co/Ni (*2c*), and Co/Ni (*3g*) sublattices is ferromagnetic, and the quality of their fit  $\chi^2$  to the observed NPD profile and PNPd (Sec. III D) refinements.

Configuration	Sign with respect to the magnetic axis			NPD, $\chi^2$	PNPD, $\chi^2$
	<i>1a</i>	<i>2c</i>	<i>3g</i>		
A	+	+	+	3.5	11.6
B	+	+	-	1.7	8.7
C	+	-	+	3	9.7
D	+	-	-	1.3	1.6

scattering, constant background), hence enhancing sensitivity to the magnetic scattering contribution compared with NPD and enabling the study of magnetic structures with small ordered magnetic moments.<sup>28–31</sup>

This technique was originally developed for the case of isotropic<sup>32</sup> (soft) ferromagnetic (ferrimagnetic) single crystals and powders<sup>28–31</sup> and locally anisotropic parameters.<sup>33</sup> In all these cases, both the bulk magnetization *M* and the incident neutron beam polarization *P* are oriented parallel to the external magnetic field *H*<sub>0</sub>. In the present work, we apply the PNPd technique to the case of highly anisotropic<sup>32</sup> (hard) ferrimagnetic powder. In this case, the magnetization direction in an individual grain depends on its crystallographic orientation with respect to the external field. As a consequence, in each grain,<sup>34</sup> only one component of the magnetization is parallel to the polarization of the neutron beam (see Appendix). The magnitude of this component varies between the grains. Therefore, conventional PNPd formulas, developed in Refs. 28–31, do not hold.

The magnitude of the anisotropy (hard or soft ferromagnet) could be determined by comparing the MCA energy with that of the magnetic energy  $\mu_B H_0$  provided by the external magnetic field. The MCA energy of TbCo<sub>5</sub> was previously determined as  $\sim 13$  meV.<sup>3</sup> The MCA in TbCo<sub>2</sub>Ni<sub>3</sub> can be estimated using the *T<sub>C</sub>* ratios between the two compounds as  $\sim 4$  meV. On the other hand, the magnetic energy  $\mu_B H_0$  for *H*<sub>0</sub> = 5 T Fig. 7(a) is equal to  $\sim 0.2$  meV. Hence, *H*<sub>0</sub> is too weak to change the magnetic structure in TbCo<sub>2</sub>Ni<sub>3</sub>.

The observed FD intensity *I*<sub>+</sub> – *I*<sub>-</sub> in powders is calculated by averaging over all grains that contribute to the *hkl* Bragg reflection (see Appendix); introducing  $\langle \cos \beta \rangle_{hkl}$  [Eq. (2)] and considering the appropriate geometrical and physical intensity corrections,<sup>28–30</sup> the calculated FD intensity is given by

$$I_+ - I_- \propto D(2\theta) T(2\theta) \langle \cos \beta \rangle_{hkl} \times \frac{e^{-2B_T \sin^2 \theta / \lambda^2}}{\sin \theta \sin 2\theta} m_{hkl} \text{Re}\{F_N F_M^\dagger\}, \quad (1)$$

TABLE IV. The PSO  $\equiv y$  and *x* dependence of the Co and Ni atoms *2c* and *3g* site occupancies in *R*(Co<sub>1-*x*</sub>Ni<sub>*x*</sub>)<sub>5</sub>. The number of ions in each site, and in the unit cell, obtained by multiplying each the site's occupancy by its respective multiplicity, is also noted.

	<i>2c</i>	<i>3g</i>	Sum
Co	(1 - <i>x</i> )(1 + <i>y</i> )	(1 - <i>x</i> )(1 - 2/3 <i>y</i> )	5(1 - <i>x</i> )
Ni	<i>x</i> - <i>y</i> + <i>y</i> <i>x</i>	<i>x</i> + 2/3 <i>y</i> - 2/3 <i>y</i> <i>x</i>	5 <i>x</i>
Sum	2	3	5

where *D*(2*θ*) is the beam depolarization inside the sample, *T*(2*θ*) is the absorption-corrected geometrical transmission function (in Debye-Scherrer geometry),<sup>20</sup> *B<sub>T</sub>* is the average (Debye-Waller) temperature factor,  $\lambda = 0.84(1)$  Å is the wavelength of the monochromatic neutron beam, *m<sub>hkl</sub>* is the *hkl* multiplicity of the Bragg reflection,  $\text{Re}\{\dots\}$  is the real part of a complex number, and *F<sub>N</sub>* and *F<sub>M</sub>* are the nuclear and magnetic structure factors, respectively. Here, *F<sub>M</sub>* includes the atomic form factors of Tb,<sup>35</sup> Co,<sup>36</sup> and Ni (Ref. 37) ions.

The magnetic information regarding the magnetic structure that is obtained using PNPd for the case of hard ferromagnetic powders [Eq. (1)] is fundamentally different from that previously reported for soft ferromagnets.<sup>28–31</sup> In addition to the magnetic configuration (i.e., the magnetic moment magnitudes and relative signs) obtained for soft ferromagnetic powder, the  $\langle \cos \beta \rangle_{hkl}$  (see Appendix) component enables one to extract  $\Theta$ .

The angular range used in the PNPd analysis is  $7^\circ < 2\theta < 30^\circ$  and contains nine Bragg reflections [Fig. 7(b)]. The angular region,  $17.5^\circ$  to  $20^\circ$ , containing the 110 reflection, is excluded from the analysis (Fig. 6) due to large statistical uncertainty which originates from the presence of a strong instrumental (cryostat, nuclear) peak. Above  $30^\circ$ , the angular resolution of the VIP diffractometer becomes too poor ( $>3^\circ$  full width at half-maximum [FWHM]). This poor angular resolution<sup>38</sup> results from the absence of angular collimation at the VIP diffractometer, which was originally designed for single crystal diffraction. In this small  $2\theta$  region (originating from the small value of  $\lambda$ ), we can neglect the  $2\theta$  dependence

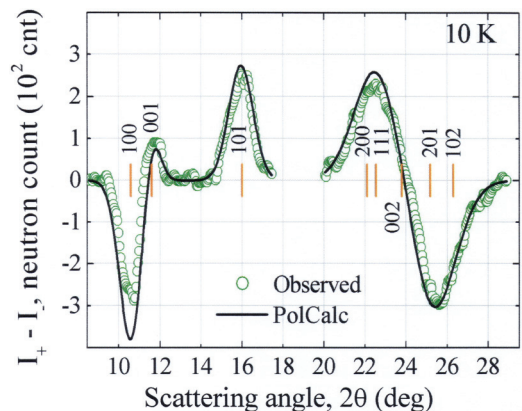


FIG. 6. (Color online) *I*<sub>+</sub> – *I*<sub>-</sub> profile of TbCo<sub>2</sub>Ni<sub>3</sub> at 10 K. The circles represent the observed PNPd profile and the solid line is the PolCalc refinement profile (see text). The reflections calculated  $2\theta$  positions are marked and their Miller (*P6/mmm*) indices are given.

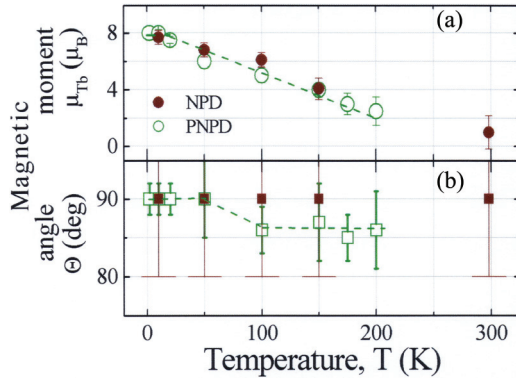


FIG. 7. (Color online) The temperature dependence of the refined (a) Tb magnetic moment,  $\mu_{Tb}$ , and (b) the magnetic axis angle  $\Theta$  with the  $c$  axis (solid symbols: NPD; open symbols: PNPd). The PNPd error bars in (b) are dominated by systematic uncertainty, while those of NPD are entirely systematic. The dashed lines are guides to the eye.

of the beam depolarization  $D$  due to the negligible difference in neutron flight paths inside the sample.

Due to the poor angular resolution, no attempt was made to use the PNPd data for refinement of the structural parameters, and they were fixed at their NPD values (Table II) throughout the PNPd analysis. The PolCalc routine<sup>39</sup> (see also Supplemental Material<sup>40</sup>) was created to refine (by iterations) the magnetic parameters until the best fit of the calculated to the observed  $I_+ - I_-$  [Eq. (1)] is achieved. Contrary to the NPD Rietveld refinement (Subsec. C), the PNPd PolCalc is carried for the integrated FD intensities of the Bragg reflections. The magnetic parameters, refined in this way, are summarized in Table V. For the purpose of display, the best fit integrated intensities are converted back into a calculated best fit PolCalc refinement profile [Figs. 7(a) and 8]. Simple Gaussian line functions are used in this conversion.

The PNPd (Table V) and NPD (Table II) refined parameters are in good agreement. In a ferromagnetic (ferrimagnetic) structure, the magnitude and orientation of the magnetic moments are deduced from the integrated intensities of

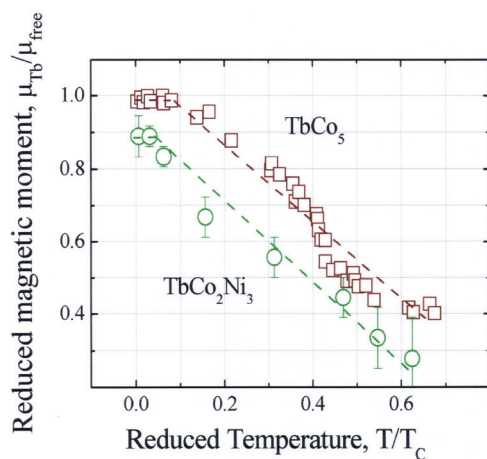


FIG. 8. (Color online)  $\mu_{Tb}/\mu_{free}$  as a function of  $T/T_C$  for  $TbCo_2Ni_3$  (circles: Table V) and for  $TbCo_5$  (squares: Ref. 42). The dashed lines are guides to the eye.

the Bragg peaks only. Moreover, the magnetic scattering contribution decreases considerably with increasing scattering vector  $K$  (due to the atomic form factor), contrary to the nuclear scattering. Hence, despite the poor angular resolution and the limited angular range (small  $hkl$ ; Fig. 6), the magnetic parameters refined from the observed PNPd data are more precise (smaller standard deviations) than those from the NPD.<sup>30</sup>

### E. Ordered magnetic moment in the Tb sublattice

The observed PNPd magnitude of  $\mu_{Tb}$  as a function of temperature agrees with that observed using NPD [Fig. 7(a)]. We note that this temperature dependence is approximately linear lacking the curvature characterizing spontaneous magnetization type behavior, considering only the MEF interaction (mean field approximation). In addition, the PNPd refined magnetic axis angle  $\Theta$  shows a small reorientation of the magnetic axis towards the hexagonal  $c$  axis [Fig. 7(b)]. Correlations between  $\Theta$  and  $\mu_{Tb}$ ,  $\mu_{2c}$ , and  $\mu_{3g}$  in the PolCalc refinement of the PNPd introduce a significant systematic component into the error of the refined  $\Theta$ . These correlations are higher in the Rietveld refinement of the NPD, causing entirely systematic  $\Theta$  errors. The small decrease in  $\Theta$  that appears in the PNPd refinement is absent in the NPD refinement, Fig. 7(b). The decrease is significant within the error of the PNPd refinement. Due to the large errors of the NPD refinement, the results of the PNPd and NPD experiments are still in agreement albeit this difference.

The reduced magnetic moment's value  $\mu_{Tb}/\mu_{free}$  in  $TbCo_2Ni_3$  (present work) as a function of the reduced temperature  $T/T_C$  (Fig. 8) is compared with this function in  $TbCo_5$ ,<sup>42</sup> where  $\mu_{free} = 9 \mu_B$  is the magnetic moment's magnitude of the free  $Tb^{3+}$  ion. Here,  $T_C = 315$  K (present work) and  $T_C = 980$  K,<sup>2</sup> for  $TbCo_2Ni_3$  and  $TbCo_5$ , respectively. There is a similarity in the  $T/T_C$  dependence of the reduced Tb magnetic moment  $\mu_{Tb}/\mu_{free}$  in  $TbCo_2Ni_3$  and  $TbCo_5$ , Fig. 8. The saturated magnetic moment is temperature independent in the low temperatures region. As the temperature is raised, the magnetic moments exhibit moderate decrease with similar slopes. Similar reduced moment  $\mu_{Er}/\mu_{free}$  vs  $T/T_C$  dependence was found in  $ErCo_2Ni_3$ .<sup>43</sup> Also, upon Ni dilution of the Co sublattices in  $TbCo_5$ , the  $\mu_{Tb}/\mu_{free}$  vs  $T/T_C$  graph shifts to smaller  $\mu_{Tb}/\mu_{free}$  and  $T/T_C$ . These suggest that the ordering mechanism of  $\mu_{Tb}$  is driven by the Co ions in the Co/Ni sublattice. A theoretical discussion of these mechanisms, as well as those responsible for the  $\Theta$  anisotropy will be given elsewhere.<sup>44</sup>

This temperature dependence is fundamentally different from the standard spontaneous magnetization curves within the mean field approximation (Sec. IV).

### F. Ordered magnetic moment in the Co/Ni sublattices

The PNPd refined ordered magnetic moments of Co/Ni ions in sites 2c and 3g are given in Table V and shown in Fig. 9(a). It was previously determined that the magnetic moments of the Co<sup>2.5</sup> and Ni<sup>1.5</sup> ions are different from each other and vary mildly with the site (i.e., 2c, 3g) they occupy. For example, the observed magnitudes of the Co ion magnetic

TABLE V. Refined PNPd magnetic parameters in the  $P1$  space group representation of  $\text{TbCo}_2\text{Ni}_3$  at temperatures  $T = 10, 50, 100, 150, 175, 200$ , and  $250$  K. The structural parameters were fixed at the values obtained with the  $10$  K NPD refinement (Table II). The refined magnetic parameters  $\mu_{\text{Tb}}$ ,  $\mu_{2c}$ , and  $\mu_{3g}$  are the ordered magnetic moments at Tb ( $1a$ ), Co/Ni ( $2c$ ), and Co/Ni ( $3g$ ) sites, respectively. Here,  $\Theta$  is the angle between the magnetic and hexagonal axes. Also, PSO is of the Co at  $2c$  (Sec. III C). The fitting criteria between the observed and calculated (using PolCalc) profiles is based on the standard  $\chi^2$  algorithm.<sup>41</sup> Numbers in parentheses are standard deviations of the last significant digit. Parameters lacking standard deviation were fixed throughout the refinement.

$T(K)$	10	20	50	100	150	175	200
Parameter							
$\mu_{\text{Tb}} (\mu_B)$	8.0(3)	7.5(3)	6.0(5)	5.0(5)	4.0(5)	3.0(8)	2.5(10)
$\mu_{2c} (\mu_B)$	-0.78(5)	-0.70(6)	-0.43(9)	-0.21(5)	-0.36(3)	-0.14(3)	-0.28(5)
$\mu_{3g} (\mu_B)$	-0.96(5)	-0.98(6)	-0.96(8)	-0.36(5)	-0.24(5)	-0.36(4)	-0.12(5)
$\Theta$ (deg)	90(2)	90(2)	90(5)	86(3)	87(5)	85(3)	86(5)
PSO	-0.29(4)	-0.29	-0.29	-0.29	-0.29	-0.29	-0.29
$\chi^2$	1.5	1.4	2.2	1.9	1.6	1.6	2.5

moments at sites  $2c$  and  $3g$  in  $\text{YCo}_5$  is  $1.77(2)$  and  $1.72(2) \mu_B$ , respectively.<sup>5</sup> Using the PNPd refined  $\text{PSO} = -0.29(4)$  value (Table V), we deduce (Table IV) Co occupancy of  $0.28(2)$  and  $0.47(3)$  at sites  $2c$  and  $3g$ , respectively. Acknowledging that, within the experimental precision in this work  $\sim 0.1 \mu_B$  (Table V), we can assume that  $\mu_{\text{Co}}$  and  $\mu_{\text{Ni}}$  are independent of the site they occupy. Hence, using the refined values  $\mu_{2c}$  and  $\mu_{3g}$ , with the respective Co and Ni site occupancies, we obtain  $\mu_{\text{Co}}$  and  $\mu_{\text{Ni}}$  as a function of temperature [Fig. 9(b)]. At low temperatures ( $T < 50$  K),  $\mu_{\text{Co}} = -1.5(5)$  and  $\mu_{\text{Ni}} = -0.6(3) \mu_B$  are in good agreement with the previously reported  $-1.7(1) \mu_B$  (Ref. 5) and  $-0.4(1) \mu_B$  (Ref. 15), obtained in  $\text{YCo}_5$  and  $\text{TbNi}_5$ , respectively. As temperature is increased,  $\mu_{\text{Ni}}$  shows very small temperature dependence, while  $\mu_{\text{Co}}$  reduces to zero (within the experimental precision).

#### IV. DISCUSSION

It is found that  $\text{TbCo}_2\text{Ni}_3$  orders at  $T_C = 315$  K in a ferrimagnetic structure consisting of ferromagnetic Tb and ferromagnetic Co/Ni sublattices. The magnetic axis at low temperatures is perpendicular to the crystallographic  $c$  axis. This result is in general agreement with the magnetic structure

found in  $\text{TbCo}_5$ ,<sup>2</sup>  $\text{TbNi}_5$ ,<sup>45</sup>  $\text{ErCo}_2\text{Ni}_3$ ,<sup>43</sup> and<sup>11</sup>  $\text{PrCo}_2\text{Ni}_3$ . (Ref. 11). The Tb contribution to the anisotropy in these compounds favors alignment of magnetic moments in the hexagonal basal plane, while that of the Co favors alignment along the hexagonal  $c$  axis.<sup>2,3</sup> The MCA energy strongly depends on the magnitude of the magnetic moments.<sup>2,3</sup> Hence, as temperature is lowered, the Tb ordered moment increases until the magnetic structure is aligned perpendicular to the crystallographic  $c$  axis below  $\sim 50$  K.

In  $\text{TbCo}_5$ , as  $T$  is increased, the magnetic axis reorients from the basal plane and becomes aligned parallel to the  $c$  axis at  $T/T_C \sim 0.5$ .<sup>2,3,42</sup> In  $\text{TbCo}_2\text{Ni}_3$ , on the other hand, as  $T$  is increased, such a realignment of the magnetic axis does not take place up to  $T/T_C \sim 0.8$  [Fig. 7(b)]. The Tb ( $1a$  site) carries the basal plane MCA (bp-MCA), whereas the Co ( $2c$  site) carries the  $c$ -MCA (Sec. I). At low temperatures, the MCA is dominated by the bp-MCA in both  $\text{TbCo}_5$  and  $\text{TbCo}_2\text{Ni}_3$ . As  $T$  is increased, the bp-MCA decreases (due to  $\mu_{\text{Tb}}$  decrease), until a temperature is reached, where the bp-MCA is smaller than the  $c$ -MCA. At this temperature,  $c$ -MCA takes over the MCA domination, eventually leading to realignment of the magnetic axis parallel to the  $c$  axis. This realignment occurs in  $\text{TbCo}_5$  at  $T/T_C \sim 0.5$ , whereas, in  $\text{TbCo}_2\text{Ni}_3$ , the Ni dilution of the Co ( $2c$  site) reduces the  $c$ -MCA to a level where it cannot dominate the MCA, so realignment is not observed up to  $T/T_C \sim 1$  Fig. 7(b).

The magnetic transition temperature  $T_C \sim 315$  K is higher than that found in  $\text{YCo}_2\text{Ni}_3$ ,  $T_C \sim 270$  K (Fig. 4). As the  $\text{Y}^{3+}$  ions are nonmagnetic, the  $45$  K increase in  $T_C$  suggests that the mechanism responsible for  $T_C$  contains magnetic interaction between the Tb and the Co/Ni sublattices.

At  $10$  K, we observed  $\mu_{\text{Tb}} = 8.1(2) \mu_B$ . This value is reduced compared to the free  $\text{Tb}^{3+}$  ion ( $9 \mu_B$ ). A reduction of this sort (in rare earth ions) in the magnetic moment was previously found when there was a competition between MEF and CEF.<sup>6</sup> Furthermore, the observed temperature dependence of the magnitude of this moment (Fig. 10) does not follow spontaneous magnetization curvature, as described within the framework of the mean field approximation.<sup>46</sup> For comparison, two spontaneous magnetization curves (Fig. 10) were calculated, within the mean field approximation,<sup>32</sup> using two sets of exchange coupling constant  $\Gamma$  multiplied by the number of nearest neighbor ions  $Z$ .<sup>32</sup> The observed temperature

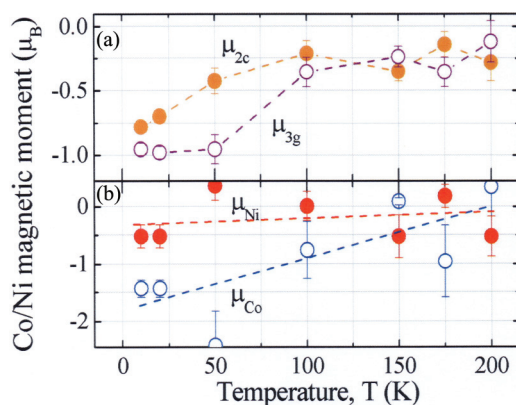


FIG. 9. (Color online) The Co/Ni ordered magnetic moments. (a) The PNPd refined values of  $\mu_{2c}$  (solid circles) and  $\mu_{3g}$  (open circles) as a function of temperature. (b)  $\mu_{\text{Co}}$  and  $\mu_{\text{Ni}}$  (derived from  $\mu_{2c}$  and  $\mu_{3g}$ , assuming they are independent of the site they occupy) as a function of temperature. The dashed lines are guides to the eye.

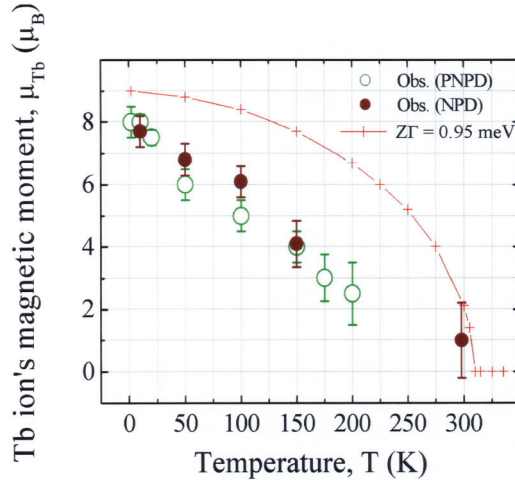


FIG. 10. (Color online) Temperature dependence of the NPD and PNPD observed  $\mu_{Tb}$  and a calculated spontaneous magnetization curve based on the mean field approximation, using the exchange coupling constant  $\Gamma$  and the number of nearest neighbor ions  $Z$ .

dependence of  $\mu_{Tb}$  exhibits two regions (Fig. 8): (i)  $0 < T < 20$  K,  $\mu_{Tb}$  is temperature independent with reduced magnitude compared to the free ion; and (ii)  $20 < T$  K approximately linear, moderate, decrease of  $\mu_{Tb}$  with increasing temperature. This temperature dependence is markedly different from that of the calculated spontaneous magnetization curve (Fig. 10), which exhibits convex and steep decrease with temperature.

A theoretical discussion of the mechanisms driving the magnetically ordered state of the Tb ions is underway,<sup>44</sup> in which the interrelation between the crystalline electric and the MEFs is taken into account. We suggest that the obtained linear temperature dependence, with a  $\sim 10\%$  reduction in the magnitude of  $\mu_{Tb}$  compared with the free  $Tb^{3+}$  ion value at low temperatures ( $T < 10$  K), is the consequence of a combined action of the crystalline electric and MEFs, similar to that previously established in  $TbCo_3B_2$ .<sup>6</sup> This combined action may lead to a self-induced magnetic transition.<sup>6,7</sup> We suggest that the possible self-induced transition characteristics (e.g., magnetic moment magnitude at low temperature, magnetic moment temperature dependence, the relation between  $T_C$  and the MEF) in these compounds are obscured by the very large MEF.

Co sublattice substitution in the ternary compounds  $R(Co_{1-x}A_x)_5$  ( $A = Ni, Fe, Al, Cu$ ) shows that the Co and A atoms are not randomly distributed between the 2c and 3g sites.<sup>6-8</sup> The NPD and the PNPD refinements yielded negative values [i.e.,  $-0.4(1)$  and  $-0.29(4)$ , respectively] for the PSO of the Co in 2c site. Hence, the Co ion clearly prefers the 3g site. This result is in agreement with the energy calculation result for  $YCo_4Ni$ ,<sup>47</sup> which showed preference for Ni occupation of the 2c site.

The PNPD analysis of powder with a hard magnetic structure, developed<sup>39</sup> and used in the present work, is fundamentally different from the commonly used PNPD analysis of powder with soft magnetic structures.<sup>28-31</sup> Considering collinear magnetic structures, the hard magnetic powder analysis enables us to extract the complete magnetic structure, that is, the magnitude and sign of the magnetic moments

and the orientation of the magnetic axis with respect to the unit cell axes. The soft ferromagnetic (ferrimagnetic) powder analysis, on the other hand, enables the extraction of the magnitude and sign of the magnetic moments (i.e., the magnetic configuration) but not the magnetic axis orientation, which is changed to coincide with the external magnetic field.

## V. CONCLUSIONS

The hexagonal  $TbCo_2Ni_3$  undergoes a magnetic phase transition at  $T_C = 315(5)$  K, below which a ferrimagnetic structure is found. The ferromagnetic Tb and the ferromagnetic Co/Ni sublattices are oppositely coupled. At  $T < 50$  K, the magnetic axis is oriented in the basal plane perpendicular to the hexagonal axis. At  $50 < T < T_C$ , a small  $2^\circ$  to  $4^\circ$  reorientation of the magnetic axis away from the hexagonal plane is observed.

The Tb ordered magnetic moment decreases linearly with temperature, similar to that of  $TbCo_5$ ,<sup>42</sup> and both do not follow spontaneous magnetization curves obtained within the mean (magnetic exchange) field approximation. In addition, the magnitude of the Tb magnetic moment at low temperature is decreased by  $\sim 10\%$  compared with that of  $TbCo_5$ .

The Ni ion preferentially occupies the 2c site with a  $\sim 20\%$  increase compared with random distribution, obtained using the (error sensitive) average between NPD and PNPD results, in agreement with energy calculations.<sup>47</sup> This significant dilution of the Co in the 2c site [occupancy =  $0.28(2)$ ] weakens considerably the c axis MCA. Hence, whereas in  $TbCo_5$  (occupancy = 1) the magnetic axis reorients upon heating (from the basal plane to the c axis at  $\sim 0.5T_C$ ) in  $TbCo_2Ni_3$ , no such reorientation is observed up to near  $T_C$ , Fig. 7(b).

The common PNPD technique is applicable to soft magnetic materials, but is not applicable to  $TbCo_2Ni_3$ , which is a hard magnetic material. A PNPD technique applicable to hard magnetic materials was developed and successfully applied in the present study.

Using results obtained in the present work (i.e., magnitude of  $\mu_{Tb}$  at low temperature,  $\mu_{Tb}$  temperature evolution  $T_C$ ), we plan to show<sup>14</sup> that the magnetic ordering transition in  $TbCo_2Ni_3$  is of the self-induced type, similar to that found<sup>13</sup> in  $TbCo_3B_2$ .

## ACKNOWLEDGMENTS

This work is partially based on experiment number 10573, performed at the Orphée research reactor at the Laboratoire Léon Brillouin, CEA—CNRS, Saclay, France. One of us (O. R.) wishes to thank E. Lelievre-Bema for his guidance in polarized scattering physics.

## APPENDIX: PNPD FOR ANISOTROPIC MAGNETIC MATERIALS

Using crystallographic symmetry considerations, each powder grain (assumed as a single crystal) is divided into magnetic domains.<sup>48</sup> In the case of hexagonal crystal, the magnetic axis can be either parallel (two magnetic domains in each powder grain) or perpendicular (six magnetic domains

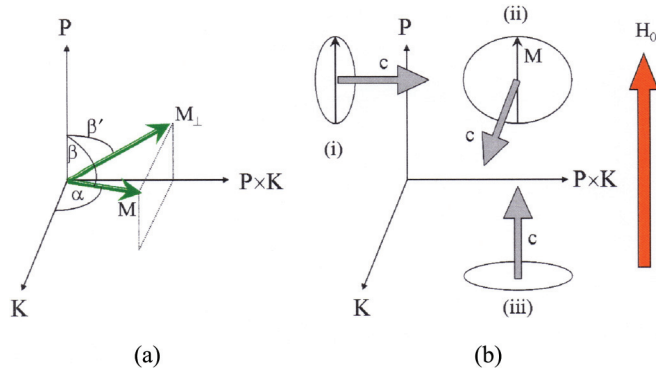


FIG. 11. (Color online) Schematic representation of (a) the vectors and angles associated with PNP scattering and (b) three groups of grains (i), (ii), and (iii), representing a very small fraction of the powder sample, and whose  $c$  axes are parallel to  $P \times K$ ,  $K$ , and  $P$ , respectively. A circle represents the easy plane ( $\Theta = 90^\circ$ ) of a grain in the group (see text). The arrow inside the circle represents the magnetization of the grain under the effect of the external field  $H_0$ .

in each powder grain) to the hexagonal axis, or a linear combination of the two cases.

In the absence of an external magnetic field, the population of the magnetic domains (i.e., their magnetic axes) is random and the net moment (powder magnetization) is zero  $\langle \cos \beta \rangle_{hkl} = 0$ , where  $\beta$  is the angle between the magnetic axis and the neutron polarization (Fig. 11). The application of an external magnetic field  $H_0$  generates a preference in the domains population  $\langle \cos \beta \rangle_{hkl} > 0$  with a mean grain magnetization  $M$  [Figs. 11(a) and 11(b)]. This preference favors domains where the magnetic axis contains a component parallel to  $H_0$  (i.e., upper hemisphere of the sphere of random distribution; Fig. 11). Nevertheless, the orientation preference of these domains is constrained by the crystallographic orientations of the powder grains, which are unaffected by the external magnetic field.

For a magnetically anisotropic hexagonal symmetry, with a considerable MCA energy difference between the hexagonal axis and the hexagonal plane, we assume a uniaxial crystal approximation,<sup>39</sup> according to which, the hexagonal plane is magnetically isotropic. Hence, we identify three cases of magnetic moment orientations with respect to the crystal axes:  $\mu \parallel c$ ,  $\mu \perp c$ , and  $\mu$  is canted with an inclination angle  $\Theta$  with respect to the hexagonal  $c$  axis. The magnetic domains population under the effect of  $H_0$ , in the special case of  $\mu \perp c$ , is schematically demonstrated in Fig. 11(b).

The contribution of a powder grain to the magnetization of the powder sample along  $H_0$  depends on its orientation in space. Let us consider, for example, the case of easy plane mode (XXZ),<sup>2,3</sup> where the magnetic axis is perpendicular to the  $c$  axis and the hexagonal symmetry is completely ignored. Let us look [Fig. 11(b)] at three groups of grains (i), (ii), and

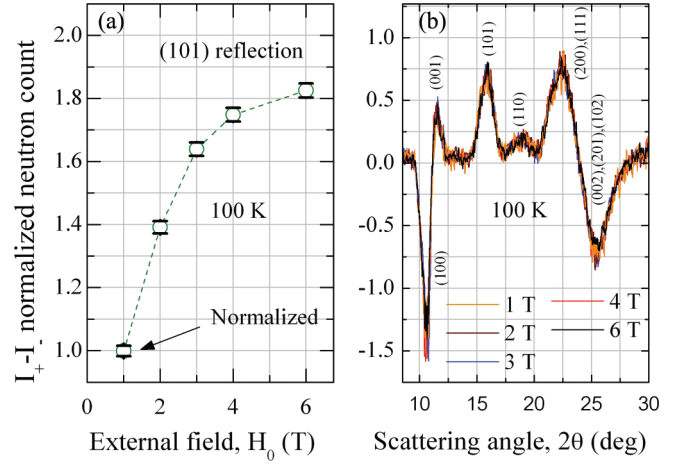


FIG. 12. (Color online) The 100 K observed (a) 101 reflection's intensity external magnetic field dependence, normalized to that observed at  $H_0 = 1$  T (the dashed line is a guide to the eye) and (b) the FD,  $I_+ - I_-$  profile, under the influence of different magnitude external magnetic fields, normalized to the 101 reflection's integrated intensity (1 T: orange, 2 T: brown, 3 T: blue, 4 T: red, and 6 T: black).

(iii), representing a very small fraction of the powder sample, whose  $c$  axes are parallel to  $P \times K$ ,  $K$ , and  $P$ , respectively. The circles perpendicular to the  $c$  axes represent the easy planes. In the case that  $H_0$  is parallel to  $P$ , all the grains with  $c$  perpendicular to  $P$  [i.e., (i) and (ii)] are completely magnetized along  $P$ . On the other hand, the grains with  $c$  parallel to  $P$  [i.e., (iii)] have no magnetization (in the first order of approximation). The powder sample contains grains whose  $c$  axes are randomly distributed in all directions. For a group of grains whose  $c$  axes are in an arbitrary direction (not shown), the circle of the easy plane is still perpendicular to the  $c$  axis, and the direction of the magnetization is in the plane of the circle and is coplanar with  $P$  and  $c$ . Using this rule,  $\langle \cos \beta \rangle_{hkl}$  is calculated<sup>39</sup> for this mode by integrating over all  $c$  directions which contribute to (the Bragg reflection)  $K$ . The result of these calculations is<sup>39</sup>

$$\langle \cos \beta \rangle_{hkl} = \frac{2}{\pi} [\cos \Theta \sin \alpha_{hkl} + \sin \Theta E(\pi/2 - \alpha_{hkl})], \quad (\text{A1})$$

where  $\alpha_{hkl}$  is the angle between the magnetic moment and the scattering vector  $K$  (Ref. 49) for the Bragg  $hkl$  reflection [Fig. 6(a)], and  $E(\pi/2 - \alpha_{hkl})$  is the complete elliptic integral of the second kind,<sup>50</sup> evaluated at  $\pi/2 - \alpha_{hkl}$ .<sup>39</sup>

The values of  $E(\pi/2 - \alpha_{hkl})$ , thus calculated, for the observed Bragg reflections [Fig. 12(b)] are presented in Table VI.<sup>39</sup>

The correction to Eq. (2) due to the finite vertical acceptance angle of  $-5^\circ$  to  $5^\circ$  about the scattering plane (Sec. II) is less than 1%.

TABLE VI. The calculated values of  $E(\pi/2 - \alpha_{hkl})$ .

$K$	100	001	101	110	200	111	002	201	102
$\alpha$	0	90	46.96	0	0	31.73	90	28.17	64.98
$E(\pi/2 - \alpha)$	1	1.571	1.368	1	1	1.227	1.571	1.194	1.498

The magnitude of the applied external magnetic field  $H_0$  is crucial to the experimental reliability. A small  $H_0$  will fail to generate measurable FD intensity (a small  $\langle \cos \beta \rangle_{hkl}$ ). A large  $H_0$  may overcome the magnetic anisotropy, thus affecting the magnetic structure. The increase of the 101 FD integrated intensity ( $\langle \cos \beta \rangle_{101}$ ) with  $H_0$  [Fig. 12(a)] shows a saturation at  $\sim 8$  T (powder saturation magnetization). No change is observed [Fig. 12(b)] in the profile of the normalized FD

intensity as the external magnetic field is increased. Thus, we conclude that the powder grain orientations are not affected, and the magnetic structure remains unchanged under the influence of the external magnetic field up to fields of 6 T, in agreement with our estimate in Sec. III D. Hence, the observed integrated FD for the 101 reflection [Fig. 12(a)] represents the powder magnetization and is proportional to the mean domains population  $\langle \cos \beta \rangle_{hkl}$ .

\*Corresponding author: lexoed@gmail.com

<sup>1</sup>E. A. Nesbitt and J. H. Wernick, *Rare Earth Permanent Magnets* (Academic Press, New York, 1973).

<sup>2</sup>Z. Tie-song, J. Han-min, G. Guang-hua, H. Xiu-feng, and C. Hong, *Phys. Rev. B* **43**, 8593 (1991).

<sup>3</sup>R. J. Radwanski, *J. Magn. Magn. Mater.* **62**, 120 (1986).

<sup>4</sup>R. L. Streever, *Phys. Rev. B* **19**, 2704 (1979).

<sup>5</sup>J. Schweizer and F. Tasset, *J. Metal. Phys.* **10**, 2799 (1980).

<sup>6</sup>O. Rivin, R. Osborn, A. I. Kolesnikov, E. N. Caspi, and H. Shaked, *Phys. Rev. B* **78**, 184424 (2008).

<sup>7</sup>B. R. Cooper and O. Vogt, *J. Phys.-Paris* **32**, 958 (1971).

<sup>8</sup>O. Moze, L. Pareti, A. Paoluzi, and K. H. J. Buschow, *Phys. Rev. B* **53**, 11550 (1996).

<sup>9</sup>C. Zlotea and O. Isnard, *J. Alloys Comp.* **346**, 29 (2002).

<sup>10</sup>D. Benea, O. Isnard, N. Coroian, and V. Pop, *J. Opt. Adv. Matr.* **10**, 1767 (2008).

<sup>11</sup>Y. C. Chuang, C. H. Wu, S. C. Chang, and T. C. Li, *J. L. Comm. Metals* **97**, 245 (1984).

<sup>12</sup>K. H. J. Buschow and M. Brouha, *J. Appl. Phys.* **47**, 1653 (1976).

<sup>13</sup>V. Crisan, V. Popescu, A. Vemes, D. Anderica, I. Bruda, and S. Cristea, *J. Alloys Comp.* **223**, 147 (1995).

<sup>14</sup>A. G. Kuchin, A. S. Ermolenko, V. I. Khrabrov, N. I. Lourov, G. M. Makarova, Y. V. Belozarov, T. P. Lapina, and Y. A. Kulikov, *J. Magn. Magn. Mater.* **238**, 29 (2002).

<sup>15</sup>F. Keyzel, doctorate thesis, Van der Waals-Zeeman Instituut Universiteit van Amsterdam, 1997.

<sup>16</sup>E. N. Caspi, H. Etedgui, O. Rivin, M. Peilstoeker, B. Breitman, I. Hershko, S. Shilstein, and S. Shalev, *J. Archae. Science* **36**, 2835 (2009).

<sup>17</sup>A. F. Andresen and T. M. Sabine, *J. Appl. Cryst.* **10**, 497 (1977).

<sup>18</sup>A. Gukasov, S. Rodrigues, J. L. Meuriot, T. Robillard, A. Sazonov, B. Gillon, A. Laverdunt, F. Prunes, and F. Coneggio, *Physica Procedia* **42**, 150 (2013).

<sup>19</sup>A. Delapalme, J. Schweizer, G. Couderchon, and R. P. de la Bathie, *Nucl. Instrum. Methods* **95**, 589 (1971).

<sup>20</sup>J. R. Carvajal, *Physica B* **192**, 55 (1993).

<sup>21</sup>M. Potter, H. Fritzsche, D. H. Ryan, and L. M. D. Cranswick, *J. Appl. Cryst.* **40**, 489 (2007).

<sup>22</sup>A. Haidar, I. Dhiman, A. Das, K. G. Suresh, and A. K. Nigam, *J. Alloys Comp.* **509**, 3760 (2011).

<sup>23</sup>R. M. Galera, S. Pizzini, J. A. Blanco, J. P. Rueff, A. Fontaine, Ch. Giorgetti, F. Baudelet, E. Dartyge, and M. F. Lopez, *Phys. Rev. B* **51**, 957 (1995);  $T_C$  at  $x = 1, 0.6, 0.4$  are reported. At  $x = 0.2$ ,  $T_C \sim 1000$  K is reported with unspecified poor accuracy and is not shown here.

<sup>24</sup>M. Dubman, E. N. Caspi, H. Etedgui, L. Keller, M. Melamud, and H. Shaked, *Phys. Rev. B* **72**, 024446 (2005).

<sup>25</sup>E. Wolfson, E. N. Caspi, H. Etedgui, H. Shaked, and M. Avdeev, *J. Phys.: Condens. Matter* **22**, 026001 (2010).

<sup>26</sup>W. Opechowski and R. Guccione, in *Magnetism*, edited by G. T. Rado and H. Suhl (Academic, New York, 1965), p. 105.

<sup>27</sup>J. Rodriguez-Carvajal, *An introduction to the program FullProf 2000*, <http://www.ill.eu/sites/fullprof/php/tutorials.html>.

<sup>28</sup>E. Lelievre-Bema, A. S. Wills, E. Bourgeat-Lami, A. Dee, T. Hansen, P. F. Henry, A. Poole, M. Thomas, X. Tonon, J. Torregrossa, K. H. Andersen, F. Bordenave, D. Jullien, P. Mouveau, B. Guerard, and G. Manzin, *Meas. Sci. Technol.* **21**, 055106 (2010).

<sup>29</sup>A. Gukasov, M. Braden, R. J. Papoular, S. Nakatsuji, and Y. Maeno, *Phys. Rev. Lett.* **89**, 087202-1 (2002).

<sup>30</sup>R. M. Moon, T. Riste, and C. Koehler, *Phys. Rev.* **181**, 920 (1969).

<sup>31</sup>P. Day, F. Herran, A. Ludi, H. U. Gudel, F. Hullinger, and D. Givord, *Helv. Chim. Acta.* **63**, 148 (1980).

<sup>32</sup>H. J. Zeiger and G. W. Pratt, *Magnetic Interactions in Solids* (Oxford University Press, Oxford, 1973).

<sup>33</sup>A. Gukasov and P. J. Brown, *J. Phys.: Condens. Matter* **22**, 502201 (2010).

<sup>34</sup>We assume that each grain consists of a multidomain single crystal.

<sup>35</sup>G. H. Lander, T. O. Brim, J. P. Desclaux, and A. J. Freeman, *Phys. Rev. B* **8**, 3237 (1973).

<sup>36</sup>R. M. Moon, *Int. J. Magn.* **1**, 219 (1971).

<sup>37</sup>H. A. Mook, *Phys. Rev.* **148**, 495 (1966).

<sup>38</sup>The angular FWHM for the VIP diffractometer is  $\sim 1.3^\circ$  at  $\sin \theta / \lambda \approx 0.2 \text{ \AA}^{-1}$ . This FWHM is two times larger than that of KARL (NPD) and four times larger than that of the High-Resolution Powder Diffractometer for Thermal Neutrons (HRPT)<sup>24</sup> (Paul Scherrer Institut, Villigen, Switzerland).

<sup>39</sup>O. Rivin, E. N. Caspi, H. Etedgui, H. Shaked, and A. Gukasov (unpublished).

<sup>40</sup>See Supplemental Material at <http://link.aps.org/supplemental/10.1103/PhysRevB.88.054430> for the average FD domains contribution for anisotropic magnetic materials.

<sup>41</sup>B. P. Roe, *Probability and Statistics in Experimental Physics* (Springer-Verlag, New York, NY, 1992).

<sup>42</sup>V. V. Kelarev, S. K. Sidorov, A. N. Pirogov, and A. P. Vokhmyanin, *Pis'ma Zh. Eksp. Teor. Fiz.* **26**, 330 (1977).

<sup>43</sup>Z. Drzazga, *Physica B* **130**, 305 (1985).

<sup>44</sup>O. Rivin, E. N. Caspi, and H. Shaked (unpublished).

<sup>45</sup>P. Dalmas de Réotier, A. Yaouanc, P. C. M. Gubbens, D. Gignoux, B. Gorges, D. Schmitt, O. Hartmann, R. Wäppling, and A. Weidinger, *J. Magn. Magn. Mater.* **104–107** (1992), and references therein.

<sup>46</sup>The mean field approximation for spontaneous magnetization is a self-consistent solution of the Brillouin response function with a permanent magnetization.<sup>32</sup>

<sup>47</sup>K. Uebayashi, K. Terao, and H. Yamada, *J. Alloys Comp.* **346**, 47 (2002).

<sup>48</sup>*International Tables for Crystallography*, Vol A, Space-Group Symmetry, edited by Th. Hahn (Kluwer, Dordercht, 1995).

<sup>49</sup>G. E. Bacon, *Neutron Diffraction*, 3rd ed. (Clarendon Press, Oxford, 1975).

<sup>50</sup>M. R. Spiegel and J. Liu, *Mathematical Handbook of Formulas and Tables*, 2nd ed. (McGraw-Hill, New-York, 1999).